IMPACT OF OXYGEN DEFICIENCY ON ELECTROCHEMICAL PERFORMANCE OF K2NiF4-TYPE (La1-xSrx)2NiO4...

Article *in* ChemSusChem · February 2017

DOI: 10.1002/cssc.201601340

CITATIONS
0

READS
69

7 authors, including:

Jekabs Grins
Stockholm University
164 PUBLICATIONS **1,767** CITATIONS
SEE PROFILE

Gunnar Svensson
Stockholm University
165 PUBLICATIONS **1,747** CITATIONS
SEE PROFILE

Vladimir Pankov
Belarusian State University
48 PUBLICATIONS **305** CITATIONS
SEE PROFILE

Aleksey Yaremchenko
University of Aveiro
187 PUBLICATIONS **4,189** CITATIONS
SEE PROFILE

CHEMISTRY & SUSTAINABILITY

CHEMSUSCHEM

ENERGY & MATERIALS

Accepted Article

Title: IMPACT OF OXYGEN DEFICIENCY ON ELECTROCHEMICAL PERFORMANCE OF K2NiF4-TYPE (La1-xSrx)2NiO4-δ OXYGEN ELECTRODES

Authors: Ekaterina Kravchenko, Kiryl Zakharchuk, Alexander Viskup, Jekabs Grins, Gunnar Svensson, Vladimir Pankov, and Aleksey A. Yaremchenko

To be cited as: *ChemSusChem* 10.1002/cssc.201601340

Link to VoR: http://dx.doi.org/10.1002/cssc.201601340

A Journal of

ChemPubSoc Europe

WILEY-VCH

www.chemsuschem.org

10.1002/cssc.201601340

IMPACT OF OXYGEN DEFICIENCY ON ELECTROCHEMICAL PERFORMANCE OF K_2NiF_4-TYPE $(La_{1-x}Sr_x)_2NiO_{4-\delta}$ OXYGEN ELECTRODES

Ekaterina Kravchenko,[a,b] Kiryl Zakharchuk,[a] Alexander Viskup,[c] Jekabs Grins,[d] Gunnar Svensson,[d] Vladimir Pankov,[b] Aleksey Yaremchenko *[a]

[a] *E. Kravchenko, K. Zakharchuk, Dr. A. Yaremchenko*
CICECO – Aveiro Institute of Materials
Department of Materials and Ceramic Engineering
University of Aveiro
3810-193 Aveiro (Portugal)
** Fax: +351-234-370204; Tel: +351-234-370235; E-mail: ayaremchenko@ua.pt*

[b] *E. Kravchenko, Prof. V. Pankov*
Department of Chemistry
Belarusian State University
Leningradskaya 14, 220006 Minsk (Belarus)

[c] *A. Viskup*
Research Institute for Physical Chemical Problems
Belarusian State University
Leningradskaya 14, 220006 Minsk (Belarus)

[d] *Dr. J. Grins, Prof. G. Svensson*
Department of Materials and Environmental Chemistry
Stockholm University
SE-106 91Stockholm (Sweden)

Abstract

Perovskite-related $(La_{1-x}Sr_x)_2NiO_{4-\delta}$ (x = 0.5-0.8) phases were explored for possible use as oxygen electrodes of solid electrolyte cells, with major focus on the effect of oxygen deficiency on electrocatalytic activity. $(La_{1-x}Sr_x)_2NiO_{4-\delta}$ solid solutions were demonstrated to preserve the K_2NiF_4-type tetragonal structure under oxidizing conditions. Acceptor-type substitution by strontium is compensated by formation of oxygen vacancies and electron-holes and progressively increases high-temperature oxygen nonstoichiometry which reaches as high as $\delta = 0.40$ for $x = 0.8$ at 950°C in air. The electrical conductivity of $(La_{1-x}Sr_x)_2NiO_{4-\delta}$ ceramics at 500-1000°C and $p(O_2) \geq 10^{-3}$ atm is *p*-type metallic-like. The highest conductivity, 300 S/cm at 800°C in air, is observed for $x = 0.6$. The average thermal expansion coefficients, $(14.0\text{-}15.4)\times10^{-6}$ K^{-1} at 25-900°C in air, are sufficiently low to ensure the thermomechanical compatibility with common solid electrolytes. The polarization resistance of porous $(La_{1-x}Sr_x)_2NiO_{4-\delta}$ electrodes applied onto $Ce_{0.9}Gd_{0.1}O_{2-\delta}$ solid electrolyte was found to decrease with increasing strontium concentration, in correlation with the concentration of oxygen vacancies in the nickelate lattice and anticipated level of mixed ionic-electronic conduction. This is accompanied however with increasing reactivity between cell components and necessitates microstructural optimization of the electrode materials to reduce electrode fabrication temperature.

1. Introduction

Lanthanum nickelate $La_2NiO_{4+\delta}$ with perovskite-related K_2NiF_4-type structure has been demonstrated to possess comparatively high electronic conductivity,[1-5] high oxygen diffusivity and surface exchange kinetics,[4-10] and moderate thermal and low chemical expansion,[3,5,11-13] and is therefore considered as a promising mixed ionic-electronic conductor (MIEC) for high-temperature electrochemical applications, such as dense MIEC membranes for oxygen separation [4,14,15] and oxygen electrodes for solid oxide fuel/electrolysis cells (SOFC/SOEC).[3,9,16-20] Good electronic transport (50-75 S/cm at 800°C in air)[1-5,21] is provided by mixed 2+/3+ oxidation state on nickel cations in perovskite layers of Ruddlesden-Popper K_2NiF_4-type structure, while ionic transport in $La_2NiO_{4+\delta}$ occurs predominantly via migration of interstitial oxygen in rock-salt-type LaO layers.[22-26] At ambient temperature, the symmetry of $La_2NiO_{4+\delta}$ crystal lattice depends on the level of frozen-in oxygen overstoichiometry δ.[27-29] Above ~450°C, the equilibrium oxygen excess decreases upon heating and on reducing oxygen partial pressure, and the tetragonal structure (space group I4/mmm) is preserved in entire existing oxygen nonstoichiometry range.[11-13,28]

Oxygen nonstoichiometry and transport properties of $La_2NiO_{4+\delta}$ can be altered by substitutions in both A and B sublattices. $(La_{1-x}Sr_x)_2NiO_{4\pm\delta}$ is probably the most studied system based on K_2NiF_4-type lanthanum nickelate. The solid solubility of strontium cations in lanthanum sublattice was reported to be limited to 75-80 at.%.[30-34] At room temperature, substitution of lanthanum by strontium results in a transition from orthorhombic to tetragonal structure [2,21] and gradual shift from oxygen hyperstochiometry to minor oxygen deficiency (Refs.[2,30-37] and Fig.S1). This is accompanied by improvement of electrical conductivity and transition from semiconducting to metallic behavior associated with increasing average oxidation state of nickel cations.[30-33,37-39] High-temperature studies of oxygen nonstoichiometry are rather desultory,[35,40-44] but suggest that Sr-rich compositions may possess non-negligible oxygen deficiency at elevated temperatures. This is also supported by the oxygen nonstoichiometry data reported for related $(Nd_{1-x}Sr_x)_2NiO_{4-\delta}$ (x = 0.5-0.8) nickelates.[45] At the same time, the reports on high-temperature transport and electrochemical properties of $(La_{1-x}Sr_x)_2NiO_{4\pm\delta}$ solid solutions are limited mainly to La-rich side of the system.

Available literature data shows that electrical conductivity of $(La_{1-x}Sr_x)_2NiO_{4\pm\delta}$ ceramics under oxidizing conditions at temperatures below 1000°C tends to increase with Sr content in the range $0 < x < 0.5$.[1,2,38,41,43,46,47] Skinner and Kilner [6,7] reported that the substitution of 5-10 at.% of lanthanum by strontium decreases oxygen tracer diffusion coefficients at 640-840°C by almost 1-2 orders of magnitude, in correlation with decreasing concentration of mobile oxygen interstitials. In agreement with that, Li et al. [48,49] demonstrated that strontium substitution results in a decline of oxygen permeation fluxes through $(La_{1-x}Sr_x)_2NiO_{4\pm\delta}$ (x = 0.05-0.10) ceramics membranes and oxygen self-diffusion coefficient in these nickelates. Vashook et al. [35] also confirmed that oxygen permeability of dense $(La_{1-x}Sr_x)_2NiO_{4\pm\delta}$ (x = 0-0.2) membranes decreases with increasing strontium content at 850-1000°C. The reports [6,7,48] disagree on the effect of substitution on the surface exchange coefficients.

There are a number of publications claiming a positive effect of strontium substitution on the electrochemical performance of $(La_{1-x}Sr_x)_2NiO_{4+\delta}$ electrodes in solid electrolyte cells. Kammer [50] studied the electrochemical activity of $(La_{1-x}Sr_x)_2NiO_{4+\delta}$ (x = 0 – 0.175) cone-shaped electrodes in contact with $Ce_{0.9}Gd_{0.1}O_{2-\delta}$ (CGO10) solid electrolyte and showed that Sr substitution decreases electrode polarization resistance (R_η) compared to undoped lanthanum nickelate. Wang et al. [51] claimed that $(La_{0.9}Sr_{0.1})_2NiO_{4+\delta}$ electrodes applied onto $Ce_{0.8}Sm_{0.2}O_{1.9}$ (SDC) solid electrolyte exhibited improved electrode properties compared to parent $La_2NiO_{4+\delta}$ under cathodic polarization conditions, but similar activity under open-circuit conditions (R_η = 1.45 Ohm cm^2 at 700°C). Shen et al. [46] demonstrated that increasing Sr content from x = 0.05 to 0.15 reduces polarization resistance of $(La_{1-x}Sr_x)_2NiO_{4+\delta}$ electrodes in contact with $La_{0.8}Sr_{0.2}Ga_{0.83}Mg_{0.17}O_{3-\delta}$ (LSGM) electrolyte from 1.01 to 0.85 Ohm cm^2 at 700°C. The positive effect of Sr substitution on electrochemical performance was attributed to a lower formation energy of interstitial oxygen in the $(La_{1-x}Sr_x)_2NiO_{4+\delta}$ lattice compared to the parent $La_2NiO_{4+\delta}$.[46]

On the contrary, Guan et al. [52] reported that electrochemical performance of $(La_{1-x}Sr_x)_2NiO_{4+\delta}$ (x = 0 – 0.2) electrodes applied onto yttria-stabilized zirconia solid electrolyte with CGO10 buffer layer progressively decreases with increasing Sr content (R_η = 0.41 Ohm cm^2 for x = 0 and 14.4 Ohm cm^2 for x = 0.2 at 700°C), and attributed this to a decline of both bulk oxygen diffusion and surface exchange rates caused by strontium substitution. Pikalova et al. [53] observed an increase of polarization resistance of $(La_{1-x}Sr_x)_2NiO_{4+\delta}$ electrodes on SDC electrolyte from 0.73 Ohm cm^2 (x = 0) to 17.7 Ohm cm^2 (x = 0.15) at 700°C, and also attributed this to a decrease of oxygen overstoichiometry and, therefore, oxygen-ion transport in nickelate phase with strontium substitution. A correlation between the concentration of mobile ionic charge carriers (interstitial oxygen or oxygen vacancies) and electrochemical activity of porous electrodes was reported also for other Ruddlesden-Popper nickelates including oxygen-overstoichiometric $La_2Ni_{1-y}Cu_yO_{4+\delta}$ and oxygen-deficient $La_4Ni_3O_{10-\delta}$-based phases.[16] Considering these observations, one may expect that increasing oxygen deficiency in Sr-rich $(La_{1-x}Sr_x)_2NiO_{4-\delta}$ at elevated temperatures should have a positive effect on mixed conductivity and electrocatalytic activity.

Thus, the present work aimed to explore $(La_{1-x}Sr_x)_2NiO_{4-\delta}$ (x = 0.5-0.8) nickelates for possible use as oxygen electrodes for solid electrolyte cells. While the major focus was on the correlation between oxygen nonstoichiometry and electrode performance, other relevant properties, including structural stability, dimensional changes and electrical conductivity, are also studied and discussed.

2. Experimental

Powders of $(La_{1-x}Sr_x)_2NiO_{4-\delta}$ (x = 0.5, 0.6, 0.7 and 0.8) were synthesized by Pechini method using La_2O_3 (Alfa Aesar, 99.9% purity), $Sr(NO_3)_2$ (Sigma Aldrich, 99% purity) and $Ni(NO_3)_2$*$6H_2O$ (Sigma Aldrich, 98% purity) as starting reagents; the procedure is detailed in the previous work.[45] The final calcination steps were performed in

flowing oxygen at 1150-1200°C for 15-30 h with repeated regrinding. The powders were compacted uniaxially under ~40 MPa and sintered in oxygen atmosphere at 1250°C for 5 h. Sintered ceramic samples were polished and cut into rectangular bars for dilatometric and electrical measurements. The experimental density of ceramics was calculated from the mass and geometric dimensions of the samples.

Room-temperature X-ray diffraction (XRD) patterns of the powdered samples were collected using PANalytical X'Pert Alpha-1 (CuKα1 radiation, 2Θ = 10-90°, step 0.02°, 5 s/step) and Rigaku D/MAX-B (CuKα radiation, 2Θ = 20-85°, step 0.02°, 5 s/step) diffractometers. Variable-temperature XRD studies were performed in air employing PANalytical X'Pert PRO MRD instrument (CuKα radiation) equipped with an Anton-Parr XRK900 reaction chamber. The patterns were recorded between room temperature and 900°C with 100°C steps, heating rate of 5°C/min between the steps, and equilibration for 10 min at each step before the actual data acquisition. Taking into account very fast equilibration kinetics on temperature cycling in air (see subsection 3.4 below), 10 min was considered sufficient time to reach a quasi-equilibrium state. Rietveld refinements of XRD data were done using Fullprof software.

Microstructural characterization of ceramic samples was performed by scanning electron microscopy (SEM, Hitachi SU-70 instrument) coupled with energy dispersive spectroscopy (EDS, Bruker Quantax 400 detector). Dilatometric studies were conducted in air at 25-1000°C with heating/cooling rate of 3°C/min using vertical Linseis L70/2001 instrument. Thermogravimetric analysis (TGA, Setaram SetSys 16/18 instrument, sensitivity 0.4 μg, initial sample weight ~0.5 g) was carried out using powdered samples in flowing air or oxygen at 25-1000°C with constant heating/cooling rate of 2°C/min or with isothermal equilibration steps. In the course of TGA studies, each dataset included equilibration of the sample with air at 950°C. The absolute oxygen content in this reference state (air, 950°C) was determined thermogravimetrically via in situ reduction to metallic Ni, coexisting with SrO and La_2O_3, in a flowing dry 10%H_2–90%N_2 gas mixture at 950-1100°C. Electrical conductivity (σ) was measured by the 4-probe DC method as function of temperature in air at 500-1000°C and as function of oxygen partial pressure at 700-900°C in the p(O_2) range from 5×10^{-4} to 1.00 atm using O_2-N_2 gas mixtures. Oxygen partial pressure in gas mixtures was monitored by electrochemical yttria-stabilized zirconia oxygen sensor.

Electrochemical characterization of $(La_{1-x}Sr_x)_2NiO_{4-\delta}$ porous electrode layers in contact with $Ce_{0.9}Gd_{0.1}O_{2-\delta}$ (CGO10) solid electrolyte was performed using symmetrical electrode/electrolyte/electrode cells. Dense CGO10 pellets were prepared using commercial powder (CGO 90/10 UHSA, Anan Kasei Co., Japan), compacted uniaxially and sintered in air at 1600°C for 5 h. As-synthesized $(La_{1-x}Sr_x)_2NiO_{4-\delta}$ powders were mixed with α-terpineol (Sigma-Aldrich) to prepare inks. The inks were brush-painted on flat surfaces of polished CGO10 pellets and sintered in oxygen for 2 h at different temperatures between 950 and 1250°C. Thickness and surface density of electrode layers were 120-150 μm and 30±4 mg/cm^2, respectively. Electrode polarization resistance in air was determined at 700-900°C employing electrochemical impedance spectroscopy (Autolab PGSTAT302 instrument with built-in FRA module,

frequency range 10 mHz – 1 MHz). Pt gauze was used as a current collector. Microstructure of porous electrodes and electrode/electrolyte interfaces were inspected by SEM/EDS.

3. Results and discussion

3.1. Phase composition and structure

XRD analysis of as-prepared $(La_{1-x}Sr_x)_2NiO_{4-\delta}$ (x = 0.5-0.8) ceramics confirmed the formation of solid solutions with perovskite-related K_2NiF_4-type tetragonal structure (space group *I*4/*mmm*) (Fig.S2). XRD patterns of most compositions showed the presence of very minor amounts of NiO impurity (tiny peaks at 2Θ = 37.3°, 43.3° and 62.9°, on the background level). These impurity peaks remained even after prolonged calcinations at 1200°C, but their intensity was less than 1% compared to intensity the strongest (*103*) reflection of the K_2NiF_4-type phase. The presence of trace amount of nickel oxide in intermediate and Sr-rich $(La_{1-x}Sr_x)_2NiO_{4-\delta}$ solid solutions was also noted in other reports.[2,30]

Increasing strontium content in the studied compositional range has comparatively minor effect on the lattice parameters and tetragonality ratio *a*/*c* (Table 1). Lattice constant *a* shows a maximum for x = 0.6, whereas parameter *c* is minimum for x = 0.7. Unit cell volume was found to decrease slightly with increasing strontium concentration in A sublattice. These observations are in agreement with the trends previously reported in literature for $(La_{1-x}Sr_x)_2NiO_{4-\delta}$ system (Refs.[30,31,33,39,54,55] and Fig.S3).

Table 1

Unit cell parameters of as-prepared $(La_{1-x}Sr_x)_2NiO_{4-\delta}$ ceramics

x	Unit cell parameters			
	a, Å	c, Å	V, Å^3	c/a
0.5	3.8271(1)	12.4562(2)	182.438(4)	3.255
0.6	3.8293(1)	12.3676(1)	181.353(3)	3.230
0.7	3.8261(1)	12.3310(3)	180.508(6)	3.223
0.8	3.8182(1)	12.3446(2)	179.962(4)	3.233

3.2. Evolution of structure with temperature

High-temperature XRD studies demonstrated that all studied nickelates preserve the same tetragonal structure at 100-900°C in air. As an example, Fig.1 shows selected XRD patterns of $(La_{0.2}Sr_{0.8})_2NiO_{4-\delta}$ ceramics; the calculated lattice parameters as function of temperature are given in Fig.S4. The absence of phase transitions in the temperature range from 25 to 1000°C was also confirmed by DSC.

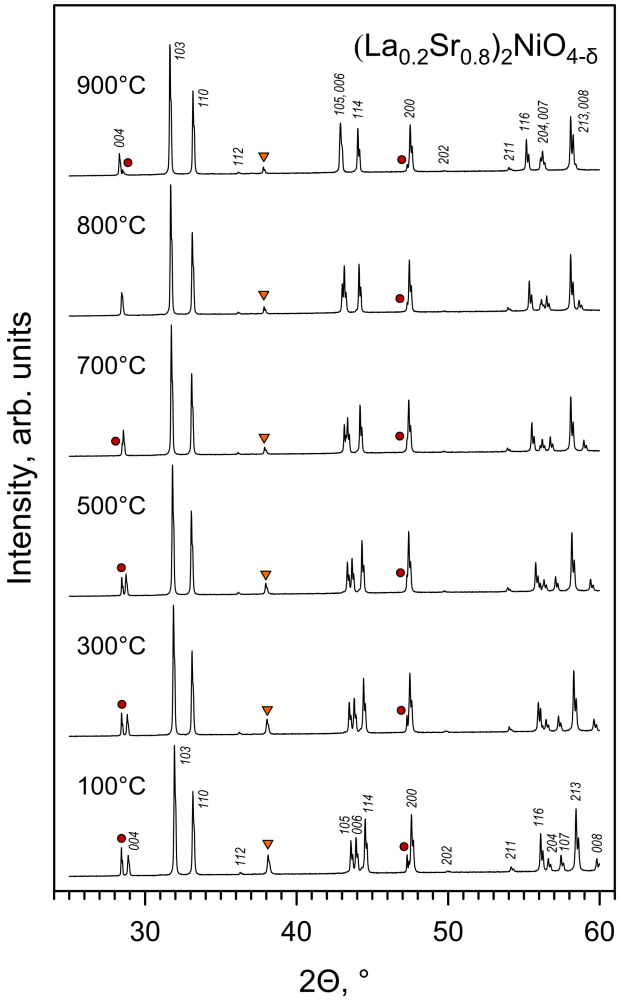

Figure 1. XRD patterns of $(La_{0.2}Sr_{0.8})_2NiO_{4-\delta}$ ceramics collected on heating in air. Reflections are indexed in the *I*4/*mmm* space group. Circles and triangles mark the peaks of Si standard and Au substrate, respectively.

All $(La_{1-x}Sr_x)_2NiO_{4-\delta}$ (x = 0.5-0.8) were found to exhibit strongly anisotropic expansion of tetragonal lattice, namely, faster elongation along *c* axis on heating if compared to *a* axis (Fig.2A and Fig.S5), in agreement with Ref.[42]. This is reflected, in particular, by a stronger shift of (*00l*) reflections in XRD patterns (Fig.1) to lower angles when temperature increases, as compared to other peaks. Furthermore, temperature dependencies of the lattice parameters progressively deviate from the linear behavior on heating leading to even stronger anisotropy of the lattice expansion at higher temperatures. The extent of these deviations correlates with Sr content and must be attributed to oxygen nonstoichiometry changes, as discussed below.

3.3. Microstructure and microcracking

Anisotropic lattice expansion introduced certain difficulties in fabrication of ceramics samples. For instance, increasing sintering temperature from 1200 to 1300°C made it possible to increase the relative density of $(La_{0.2}Sr_{0.8})_2NiO_{4-\delta}$ ceramic samples from 75 to 86% (Table 2). This was accompanied however with a noticeable grain

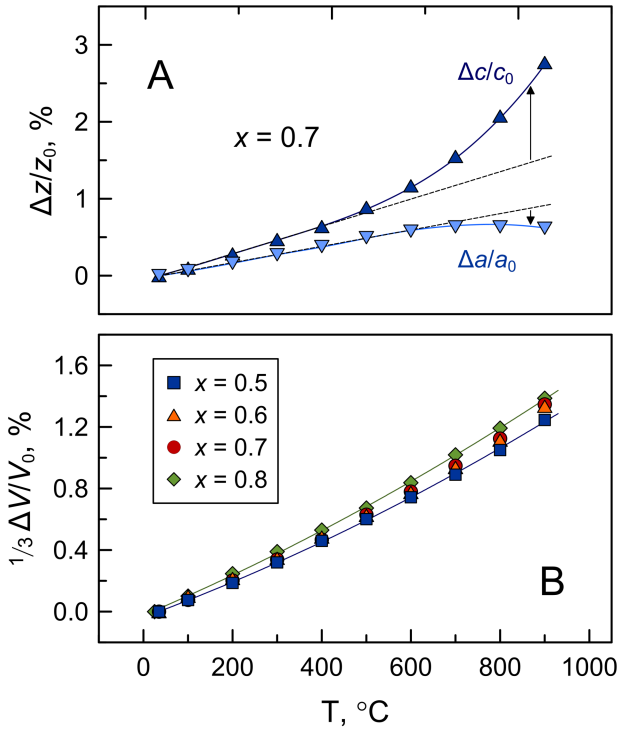

Figure 2. Relative changes of lattice parameters (A) and unit cell volume (B) of perovskite-related $(La_{1-x}Sr_x)_2NiO_{4-\delta}$ on heating in air.

growth (Fig.3(A and B) and Table 2). Grain growth, in turn, promoted microcracking inside the grains and along the grain boundaries (Fig.3C). Microcracking is a well-known phenomenon for oxide ceramic materials with crystallographic anisotropy of expansion coefficients; typical examples include Al_2TiO_5 [56] and some perovskite-like rare-earth manganites $LnMnO_3$ (e.g. Ref.[57]). Intragranular and intergranular microcracking occurs in ceramics on cooling from the sintering temperature to compensate the internal stresses induced by anisotropic shrinkage of statistically oriented grains. Increasing sintering temperature to 1350-1400°C further promoted grain growth and crack formation. As a result, the samples sintered at 1400°C retained the shape when removed from the furnace, but crumbled into a powder on touch.

Therefore, the final sintering conditions were selected to be 1250°C for 5 h, in order to provide a reasonable compromise between porosity and mechanical strength. Ceramic samples sintered in this way were comparatively porous (Fig.S6), with relative density 74-79% of theoretical (Table 2). These samples were used for dilatometric and electrical measurements. Although grain size range changes only slightly with composition (Table 2), the average grain size generally increases with strontium content (Fig.S6).

Sintered ceramics samples demonstrated a rather unusual dilatometric behavior originating from microcracking phenomenon. This includes some shrinkage on heating above 600-700°C, not completely reversed expansion on cooling below 800°C, overall hysteresis in dilatometric curves, and slow final dimensional relaxation on cooling below 100°C

(Fig.S7). The contraction on heating above 600°C is caused by a closure, or "healing", of microcracks, and dilation on cooling below 800°C is due re-cracking.[58] Once again, the extent of dimensional changes at 600-900°C correlates with the strontium content and, therefore, with anisotropicity of lattice expansion. One should stress, though, that the microcraking-related factors are not expected to be critical for mechanical behavior of porous electrode layers (with smaller grains and larger fraction of pores).

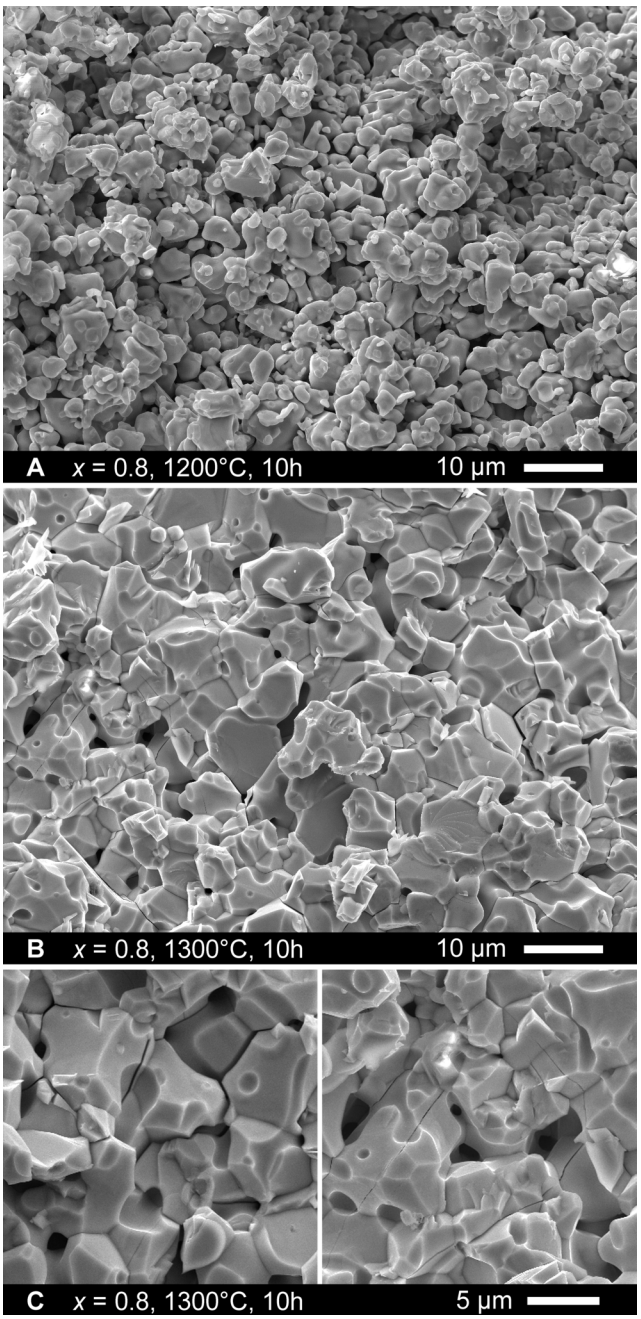

Figure 3. SEM micrographs of fractured surface of $(La_{0.2}Sr_{0.8})_2NiO_{4-\delta}$ ceramics sintered at 1200°C (A) and at 1300°C (B,C). Micrograph (C) illustrates intergranular and intragranular microcracks.

Table 2

Density and grain size of $(La_{1-x}Sr_x)_2NiO_{4-\delta}$ ceramics

x	Sintering	Grain size, μm	Density, g/cm^3	Relative density, %
0.5	1250°C, 5 h	0.8 – 7.0	4.67	74
0.6	1250°C, 5 h	0.8 – 5.0	4.69	76
0.7	1250°C, 5 h	0.9 – 9.0	4.75	79
0.8	1100°C, 10 h	0.8 – 7.0	4.09	70
	1200°C, 10 h	0.8 – 7.0	4.41	75
	1250°C, 5 h	0.7 – 7.5	4.38	75
	1300°C, 10 h	1.5 – 12.0	5.02	86

3.4. Oxygen nonstoichiometry

The results of thermogravimetric studies demonstrated that the composition with highest strontium content, x = 0.8, remains oxygen-deficient even in low-temperature range under oxidizing conditions, whilst other nickelates tend to oxygen stoichiometry below a certain temperature (Fig.4). The onset of oxygen losses from crystal lattice on heating shifts to a lower temperature with increasing strontium concentration: from 660-700°C for x = 0.5 to 270-300°C for x = 0.8. In high-temperature range, the equilibrium between nickelate crystal lattice and gas phase is described by reaction

$$2Ni_{Ni}^{(n+1)+} + O_O^{2-} \Leftrightarrow 2Ni_{Ni}^{n+} + V_O + 0.5O_2 \quad (1)$$

Oxygen deficiency increases with increasing temperature and strontium content and with reducing oxygen partial pressure (Fig.4). For $(La_{0.2}Sr_{0.8})_2NiO_{4-\delta}$, the concentration of oxygen vacancies reaches more than 10% of regular oxygen sites in tetragonal lattice at 1000°C in air. One should stress also that oxygen vacancy concentration in this material at 750-950°C in air is 2.5-4.7 times higher compared to the concentration of interstitial oxygen ions in undoped $La_2NiO_{4+\delta}$ under identical conditions.[22,40] Another comment is that all studied materials demonstrated very fast equilibration kinetics in air, with a negligible hysteresis in δ values on heating/cooling cycles with a constant rate and nearly instant stabilization of oxygen nonstoichiometry after step-wise temperature change; some examples are illustrated in Fig.S8. As a result, the values of δ obtained in dynamic cooling regime and after equilibration at each temperature at 700-950°C were equal, within experimental uncertainty (Fig.4, bottom).

Acceptor-type substitution of lanthanum by strontium in $La_2NiO_{4+\delta}$ may be compensated by changing the concentration of oxygen defects (interstitial oxygen ions or vacancies in the oxygen sublattice), or by generation of electron-holes, or both.[30,31,39,45] Interstitial oxygen can be neglected in Sr-rich $(La_{1-x}Sr_x)_2NiO_{4-\delta}$, and the electroneutrality condition is expressed by (using Kröger-Vink notation):

10.1002/cssc.201601340

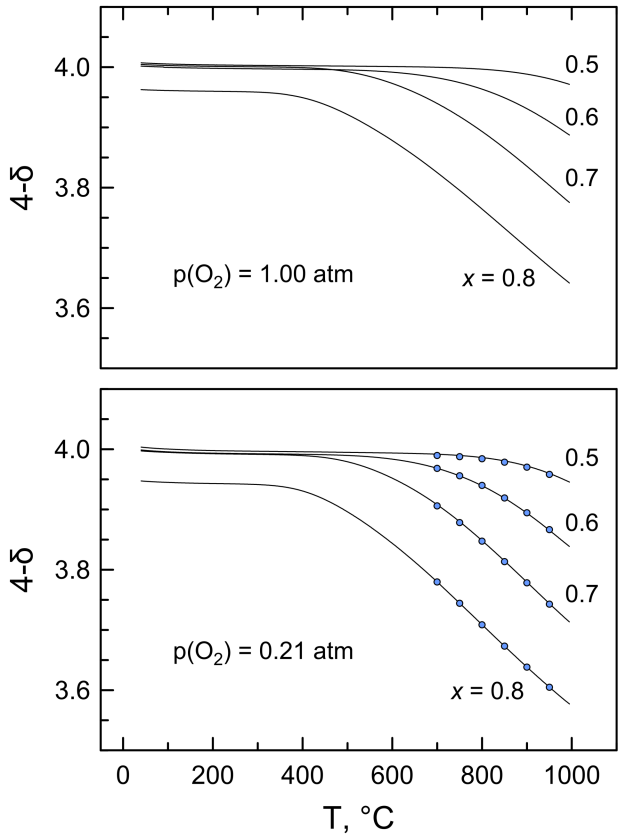

Figure 4. Temperature dependence of oxygen nonstoichiometry of perovskite-related $(La_{1-x}Sr_x)_2NiO_{4-\delta}$ in oxygen (top) and in air (bottom). Solid lines shows the data obtained at constant cooling rate of 2°C/min; circles correspond to the data obtained on stepwise cooling with equilibration for 5 h at each temperature.

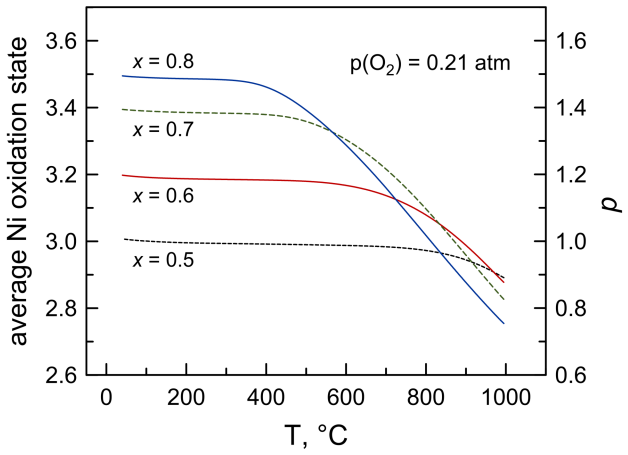

Figure 5. Temperature dependence of formal average oxidation state of nickel cations and electron-hole concentration in $(La_{1-x}Sr_x)_2NiO_{4-\delta}$ in air estimated assuming that oxygen ions are doubly charged.

$$[Sr'_{La}] = [Ni^{\bullet}_{Ni}] + 2[Ni^{\bullet\bullet}_{Ni}] + 2[V^{\bullet\bullet}_{O}] \quad (2)$$

or

$$2x = p + 2\delta \quad (3)$$

where p is the concentration of electron-holes (per formula unit) formally residing on nickel cations, i.e. $Ni^{\bullet}_{Ni} \equiv Ni^{3+}$ and $Ni^{\bullet\bullet}_{Ni} \equiv Ni^{4+}$. Analysis of the nonstoichiometry data (Fig.4) indicates that the substitution of lanthanum by strontium is compensated by generation of both oxygen vacancies and electron-holes (depending on temperature). Assuming that oxygen ions are doubly-charged, simple estimations (Fig.5) show that nickel cations are in mixed 2+/3+ oxidation state in air at high temperatures and in 4+/3+ mixed state in low-temperature range (except for x = 0.5 composition which has prevailing Ni^{3+} state below ~700°C). Oxygen losses on heating result in a decline of electron-hole concentration and in inversion of its compositional dependence: p increases with strontium content at ≤ 500°C, but decreases with increasing x at 1000°C.

3.5. Electrical conductivity

Electrical conductivity of $(La_{1-x}Sr_x)_2NiO_{4-\delta}$ ceramics in air was measured on stepwise cooling with equilibration at each step (until the drift of conductivity values with time became negligible). All prepared $(La_{1-x}Sr_x)_2NiO_{4-\delta}$ ceramics were found to exhibit comparatively high metallic-like conductivity under ambient oxygen pressure (Fig.6). Metallic-like conduction in $Ln_{2-x}Sr_xNiO_{4\pm\delta}$ is believed to occur via free electron-holes in the $\sigma_{x^2-y^2}$ band formed by delocalized $d_{x^2-y^2}$ Ni orbitals, while d_{z^2} electrons are localized.[1,30,31,54] Heating results in a decrease of both charge carrier

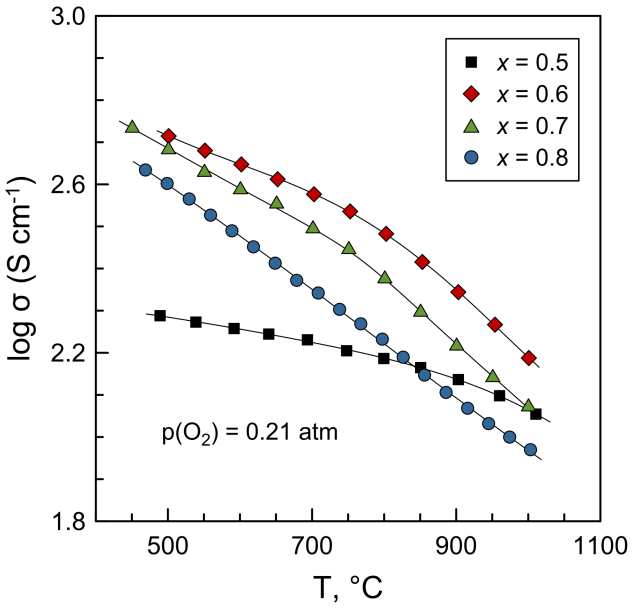

Figure 6. Temperature dependence of electrical conductivity of $(La_{1-x}Sr_x)_2NiO_{4-\delta}$ ceramics in air.

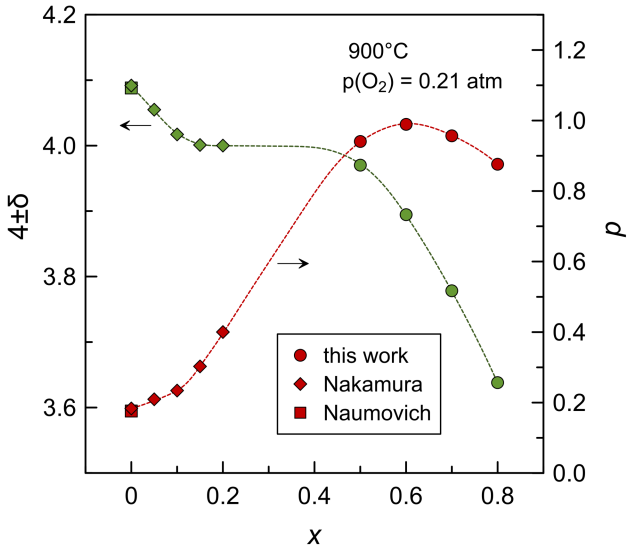

Figure 7. Dependence of oxygen nonstoichiometry and calculated electron-hole concentration in $(La_{1-x}Sr_x)_2NiO_{4\pm\delta}$ system on strontium content at 900°C in air. Oxygen nonstoichiometry data on La-rich compositions are taken from Nakamura et al. [40] and Naumovich et al.[22] The dotted lines are a guide for an eye.

concentration (Fig.5) and their mobility μ_p (partly due increasing oxygen deficiency and, therefore, increasing concentration of broken Ni-O chains in basal plane) and thus leads to a decline of conductivity.

In the $(La_{1-x}Sr_x)_2NiO_{4-\delta}$ (x = 0.5-0.8) series, electrical conductivity initially increases with strontium content reaching maximum for x = 0.6 (300 S/cm at 800°C) and then decreases on further substitution. This is in agreement with expectations based on the variations of charge-carrier concentration as function of strontium content in high-temperature range (Figs.5 and 7). Figs.S9 and S10A compare the results obtained in the present work with available literature data [1,2,38,41-43,46,47] on high-temperature electrical conductivity of $(La_{1-x}Sr_x)_2NiO_{4-\delta}$ ceramics. Generally, the data reported in literature fit the expected dependence of conductivity on composition in this system (Fig.7), but show significant scattering in absolute conductivity values. Most likely, the latter should be attributed mainly to a combination of ceramic processing-related factors (porosity, microstructural morphology and microcracking effects).

At first glance, ceramics with x = 0.5 exhibit a peculiar behavior: much weaker dependence of electrical conductivity on temperature compared to other compositions (Fig.6). One should point, however, that this correlates with the data on temperature dependencies of oxygen nonstoichiometry (Fig.4) and electron-hole concentration (Fig.5) in the $(La_{1-x}Sr_x)_2NiO_{4-\delta}$ (x = 0.5-0.8) system. For better illustration, Fig.8 shows relative variations of electron-hole concentration and electrical conductivity on heating. Being a function of charge carrier concentration, the conductivity shows qualitatively similar relative variations with temperature and composition, although its absolute values are also affected by temperature-dependent mobility and microstructural factors. In other words, increasing strontium content

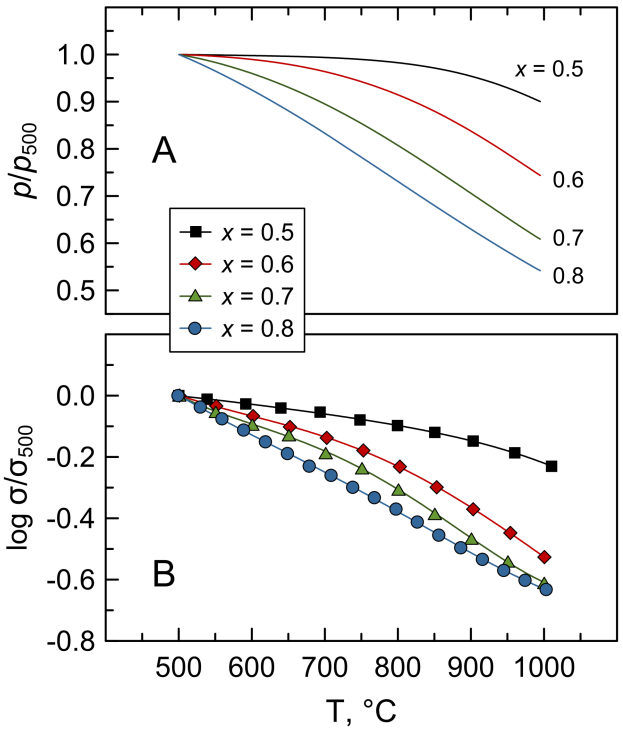

Figure 8. Relative variations of electron-hole concentration (A) and electrical conductivity (B) in $(La_{1-x}Sr_x)_2NiO_{4\pm\delta}$ system on heating in air. p_{500} and σ_{500} are charge-carrier concentration and conductivity at 500°C.

promotes stronger dependence of oxygen nonstoichiometry and, consequently, electron-hole concentration and electrical conductivity on temperature.

Electrical conductivity of $(La_{1-x}Sr_x)_2NiO_{4-\delta}$ ceramics was found to decrease on reducing oxygen partial pressure (Fig.9), thus confirming that electrical transport is *p*-type. As on heating in air, this occurs due to oxygen losses from the lattice with decreasing $p(O_2)$ accompanied by elimination of electron-holes. Redox reaction eq.(1) can be rewritten (using Kröger-Vink notation) as

$$2h^{\bullet} + O_O^{\times} \xleftrightarrow{K_{red}} V_O^{\bullet\bullet} + 0.5O_2 \qquad (4)$$

with corresponding temperature-dependent equilibrium constant

$$K_{red} = \frac{\delta}{4-\delta}\frac{p(O_2)^{1/2}}{p^2} \qquad (5)$$

Thus, *p*-type conductivity of $(La_{1-x}Sr_x)_2NiO_{4-\delta}$ ceramics is a function of oxygen partial pressure and $p(O_2)$-dependent oxygen nonstoichiometry

$$\sigma_p = e\mu_p p = e\mu_p \left(\frac{\delta}{4-\delta}\right)^{0.5} K_{red}^{-0.5} p(O_2)^{1/4} \qquad (6)$$

and shows non-linear behavior in *log σ – log p(O₂)* coordinates. Again, higher strontium content results in a stronger dependence of electrical conductivity on oxygen partial pressure (Fig.9A); this seems to indicate also increasing

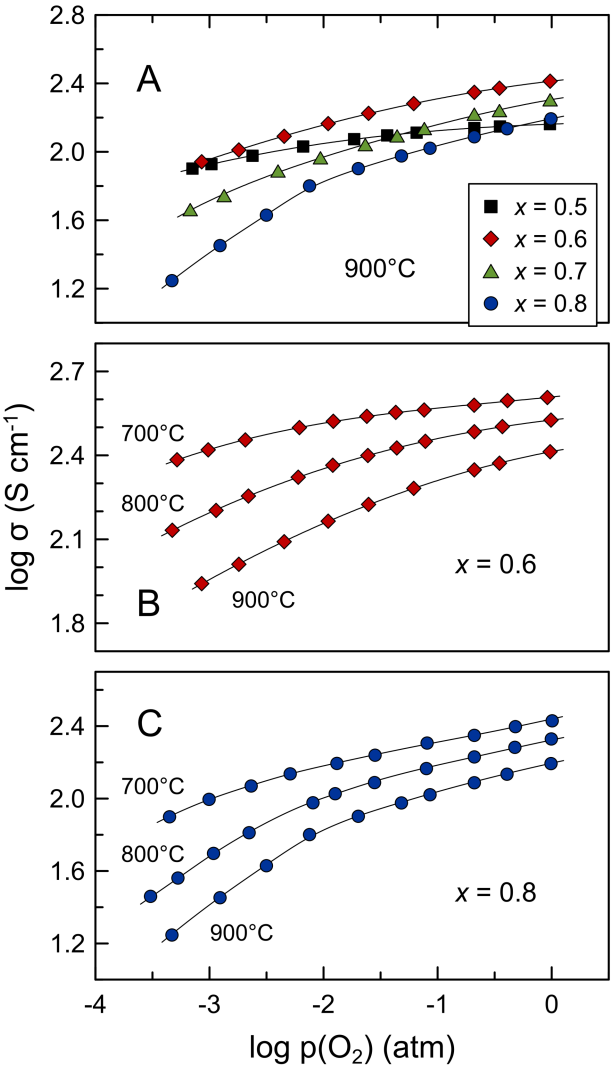

Figure 9. Oxygen partial pressure of electrical conductivity of $(La_{1-x}Sr_x)_2NiO_{4-\delta}$ ceramics: different compositions at 900°C (A), and ceramics with $x = 0.6$ (B) and $x = 0.8$ (C) at 700-900°C.

variations of δ with $p(O_2)$, in correlation with the data on heating in air (Figs.4 and 8). In the studied oxygen partial pressure range, all materials preserve metallic-like conductivity which decreases on heating, but remains sufficiently high for electrode applications (> 20 S/cm at $p(O_2) \geq 10^{-3}$ atm and 900°C even for $x = 0.8$) (Fig.9(B and C)). Comparison with available literature data for $x = 0.5$ composition reveals again large scatter of absolute conductivity values but similar shape of *log σ – log p(O₂)* curves (Refs.[59,60] and Fig.S10B)

One should stress also that noticeable oxygen deficiency in Sr-rich $(La_{1-x}Sr_x)_2NiO_{4-\delta}$ at elevated temperatures in combination with substantial electronic transport implies that these materials are mixed conductors with anticipated significant contribution of oxygen-ion transport to the total conductivity. To our knowledge, so far there is no direct experimental data confirming high mobility of oxygen vacancies in the perovskite-type layers of oxygen-deficient K_2NiF_4-type nickelates and related oxides. Nevertheless, static lattice and molecular dynamics simulations suggest

possible non-negligible contribution of oxygen vacancy diffusion in perovskite layers to overall oxygen transport even in undoped and B-site substituted $La_2NiO_{4+\delta}$.[23,61] Furthermore, combined energy minimization and molecular dynamics study of oxygen migration mechanisms in related K_2NiF_4-type $(La_{1-x}Sr_x)_2CoO_{4\pm\delta}$ predict that oxide-ion transport in oxygen-deficient $(La_{0.4}Sr_{0.6})_2CoO_{4-\delta}$ mainly occurs through migration of oxygen vacancies within the perovskite layers of the structure, although calculated oxygen diffusion coefficients are slightly lower compared to oxygen-excessive $(La_{0.6}Sr_{0.4})_2CoO_{4+\delta}$ with predominant interstitial oxygen transport.[62]

3.6. Thermochemical expansion

As pointed above, $(La_{1-x}Sr_x)_2NiO_{4-\delta}$ nickelates exhibit strongly anisotropic expansion of crystal lattice. Furthermore, increasing temperature results in a deviation of temperature dependences of lattice constants from the linear behavior (Fig.2A and Fig.S5). The extent of this deviation increases with strontium content and is in direct correlation with oxygen nonstoichiometry changes (Fig.4). In low-temperature range, when oxygen content in the lattice is constant, lattice parameters demonstrate linear variations with temperature. This can be assigned to the true thermal expansion of the lattice. Increasing oxygen deficiency in high-temperature range induces stronger elongation along *c* axis, but suppresses expansion along *a* axis and even results in some shrinkage in *a*-*b* plane for Sr-rich compositions. The latter must be attributed to chemical contribution to overall thermal expansion.

Chemical expansion (or contraction), also referred to as “stoichiometric expansion”, may occur in oxides containing variable-valence cations in response to a change in the composition, namely, in oxygen nonstoichiometry. This phenomenon originates from two simultaneous competing processes.[63,64] Formation of oxygen vacancy in crystal lattice results in a lattice contraction due to electrostatic interactions. The accompanied reduction of variable-valence metal cation results in an increase of cation radius and consequently lattice expansion due to steric effects. Typically, the latter process has a stronger impact, and oxygen losses from the lattice on heating or reducing oxygen partial pressure result in overall expansion of crystal lattice in the case of fluorite and perovskite-type oxides.[63-65]

It turns out that, in the case of K_2NiF_4-type $(La_{1-x}Sr_x)_2NiO_{4-\delta}$ tetragonal lattice, the two contributions of chemical expansion have different impact in different crystallographic directions. This is caused, apparently, by predominant formation of oxygen vacancies in NiO_2 plain, in equatorial O1 crystallographic positions (see representation of K_2NiF_4-type structure in Refs.[9,23]). The latter is in agreement with the Rietveld refinement results obtained in this work (Fig.S11), and also is supported by in situ neutron diffraction studies of oxygen-deficient Ruddlesden-Popper $(La,Sr)_{n+1}(Co,Fe)_nO_{3n+1-\delta}$,[66] and by the computer simulations of oxygen-deficient Sr-rich $(La_{1-x}Sr_x)_2MO_{4-\delta}$ (M = Co, Ni, Cu) which demonstrated prevailing oxygen transport via oxygen vacancy diffusion between equatorial O1 position in perovskite layers.[25,62] As expected, reduction of nickel cations on heating and increase of their radii contribute to elongation of axial Ni-O2 bonds (Fig.S11) and results in chemical expansion along *c* axis (Fig.2A). On the contrary,

Table 3

Average linear thermal expansion coefficients of $(La_{1-x}Sr_x)_2NiO_{4-\delta}$ in air

x	True thermal expansion coefficient, ppm K^{-1}						Thermochemical expansion $\bar{\alpha}(V^{1/3})$, ppm K^{-1} (25-900°C)
	HT-XRD				Dilatometry *		
	T, °C	$\bar{\alpha}(a)$	$\bar{\alpha}(c)$	$\bar{\alpha}(V^{1/3})$	T, °C	$\bar{\alpha}$	
0.5	25-600	9.2	23.1	13.1	120-600	11.9	14.0
0.6	25-500	9.7	20.2	13.2	120-550	12.6	14.8
0.7	25-400	10.4	17.8	12.8	120-550	13.4	15.1
0.8	25-200	13.6	15.0	14.1	120-450	14.1	15.4

* calculated from the data on heating (Fig.S7).

prevailing formation of oxygen vacancies in perovskite planes promotes shrinkage of average equatorial Ni-O1 bond length and chemical contraction along *a* axis at elevated temperatures.

In spite of crystallographic anisotropy, volume expansion of $(La_{1-x}Sr_x)_2NiO_{4-\delta}$ lattice shows nearly linear dependence in the studied temperature range (Fig.2B). This allows one to calculate average linear thermal expansion coefficients (TECs) to assess the thermomechanical compatibility with solid electrolytes. Table 3 summarizes true thermal expansion coefficients calculated from the XRD and dilatometric data in the low-temperature range (when oxygen content is constant and the dependencies are linear), and thermochemical expansion coefficients in the entire temperature range. Interestingly, increasing strontium content suppresses the anisotropy of true lattice thermal expansion, whilst average true TEC values, $\bar{\alpha}(V^{1/3})$, show rather minor variations with composition and also are close to those calculated from dilatometric data. Average thermochemical expansion coefficients values calculated from the high-temperature XRD data at 25-900°C increase slightly with *x* (Table 3) and also are comparable to TECs reported in literature for $(La_{1-x}Sr_x)_2NiO_{4-\delta}$ ceramics.[2,47,51,67] These average values exceed to some extent corresponding TECs of common solid electrolytes such as stabilized zirconia or doped ceria and lanthanum gallate,[17,65] but still seem to be low enough to ensure thermomechanical compatibility with electrolyte ceramics. At the same time, possible stresses associated with anisotropic expansion are expected to be accommodated by pores in porous electrode layers.

3.7. Electrochemical behavior of $(La,Sr)_2NiO_{4-\delta}$ electrodes

Preliminary electrochemical characterization of porous $(La_{1-x}Sr_x)_2NiO_{4-\delta}$ electrode layers were performed using CGO10 as solid electrolyte and symmetrical cell configuration. The electrodes were prepared using as-synthesized powders (calcination temperature 1150-1200°C). As a result, electrode sintering temperature (T_{sint}) had rather negligible

effect on the electrode particle size. All prepared electrodes had comparable microstructures (Fig.S12); overview of typical porous electrode layer on CGO10 electrolyte is illustrated by Fig.10A. Fig.10B shows typical impedance spectrum of symmetrical cell with equivalent circuit used for fitting and corresponding fitting results. Polarization resistance (R_η) was studied in air as function of temperature and nickelate composition (T_{sint} = 1000°C and 1100°C), and as function of sintering temperature for x = 0.8.

Decreasing electrode sintering temperature from 1250°C to 1000°C was found to reduce area-specific polarization resistance of $(La_{0.2}Sr_{0.8})_2NiO_{4-\delta}$ electrodes from 9.0 to 0.23 Ohm cm^2 at 900°C (Fig.11A). As microstructural effects were expected to be minor, electrode/electrolyte interfaces were inspected for possible interaction between electrode and electrolyte materials. Combined SEM/EDS gave clear indication of strong Sr diffusion from the electrode into the surface layer of CGO solid electrolytes (Fig.S13). No evidence of simultaneous non-negligible interdiffusion of other elements could be detected, within the accuracy of technique. The results suggest

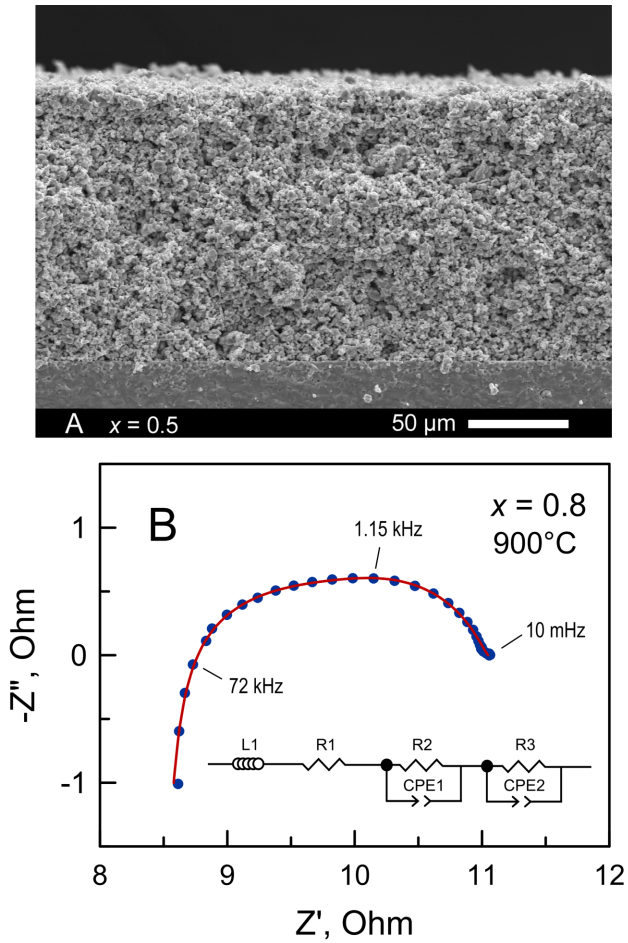

Figure 10. (A) Cross-section of $(La_{1-x}Sr_x)_2NiO_{4-\delta}$ electrode applied onto CGO10 solid electrolyte (x = 0.5, T_{sint} = 1100°C), and (B) typical impedance spectrum of $(La_{1-x}Sr_x)_2NiO_{4-\delta}$/CGO10/$(La_{1-x}Sr_x)_2NiO_{4-\delta}$ symmetrical cell collected at 900°C (x = 0.8, T_{sint} = 1000°C) with equivalent circuit used for fitting (circles are experimental data, red line is fitting results, R1 is ohmic resistance, and R2+R3 is total polarization resistance R_η).

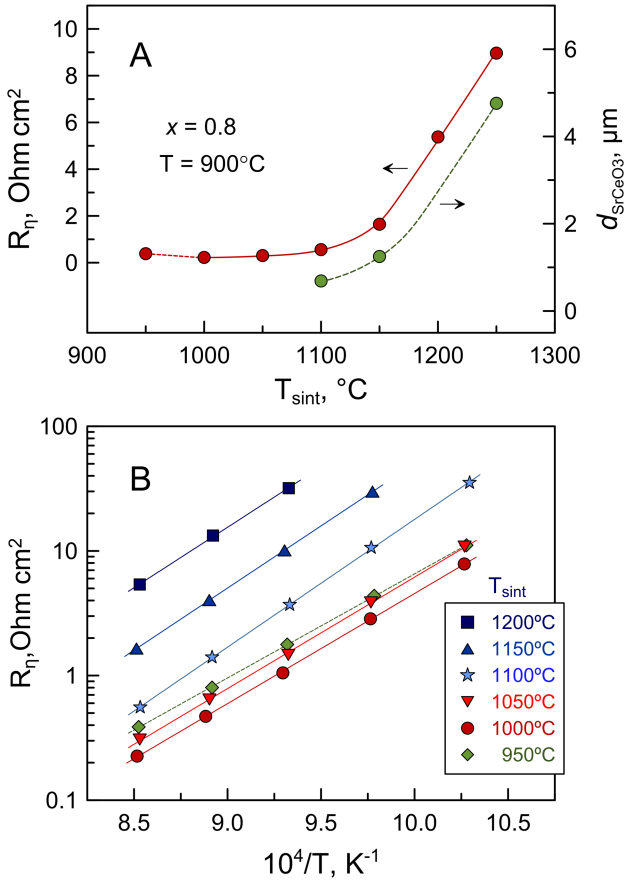

Figure 11. (A) Area-specific polarization resistance of $(La_{0.2}Sr_{0.8})_2NiO_{4-\delta}$ electrodes and average thickness (d) of $SrCeO_3$ layer at the electrode/electrolyte interface as function of electrode sintering temperature; (B) temperature dependence of polarization resistance of $(La_{0.2}Sr_{0.8})_2NiO_{4-\delta}$ electrodes sintered at different temperatures.

that interaction between electrode and electrolyte materials in the course of electrode sintering results in formation of dense layer of $SrCeO_3$-based perovskite at the electrode-electrolyte interface. The reacted area is visible as a purple layer in SEM micrographs with overlaid elemental maps of cerium and strontium (Fig.S13 and Fig.12). Apparently, strontium diffusion from the electrode into electrolyte is accompanied with the alteration of electrode material cation composition near the interface yielding La-enriched nickelate and NiO particles.

High-temperature reactivity between $(La_{1-x}Sr_x)_2NiO_{4-\delta}$ and CGO10 with formation of orthorhombic $SrCeO_3$-based perovskite phase and partial exsolution of NiO (to maintain cation stoichiometry in K_2NiF_4-type phase) was confirmed by XRD analysis of powdered mixtures calcined at 1000-1100°C (Fig.13). These results provide a clear evidence that the reactivity increases with increasing temperature and strontium content in $(La_{1-x}Sr_x)_2NiO_{4-\delta}$ electrode material.

Perovskite-type $SrCeO_3$ has rather poor transport properties if compared to CGO10 and is either electronic conductor (undoped, in dry air) or protonic conductor (acceptor doped, in wet or in H_2-containing atmospheres) (e.g. Ref.[68] and references therein). As a result, reaction between electrode and electrolyte and formation of $SrCeO_3$

10.1002/cssc.201601340

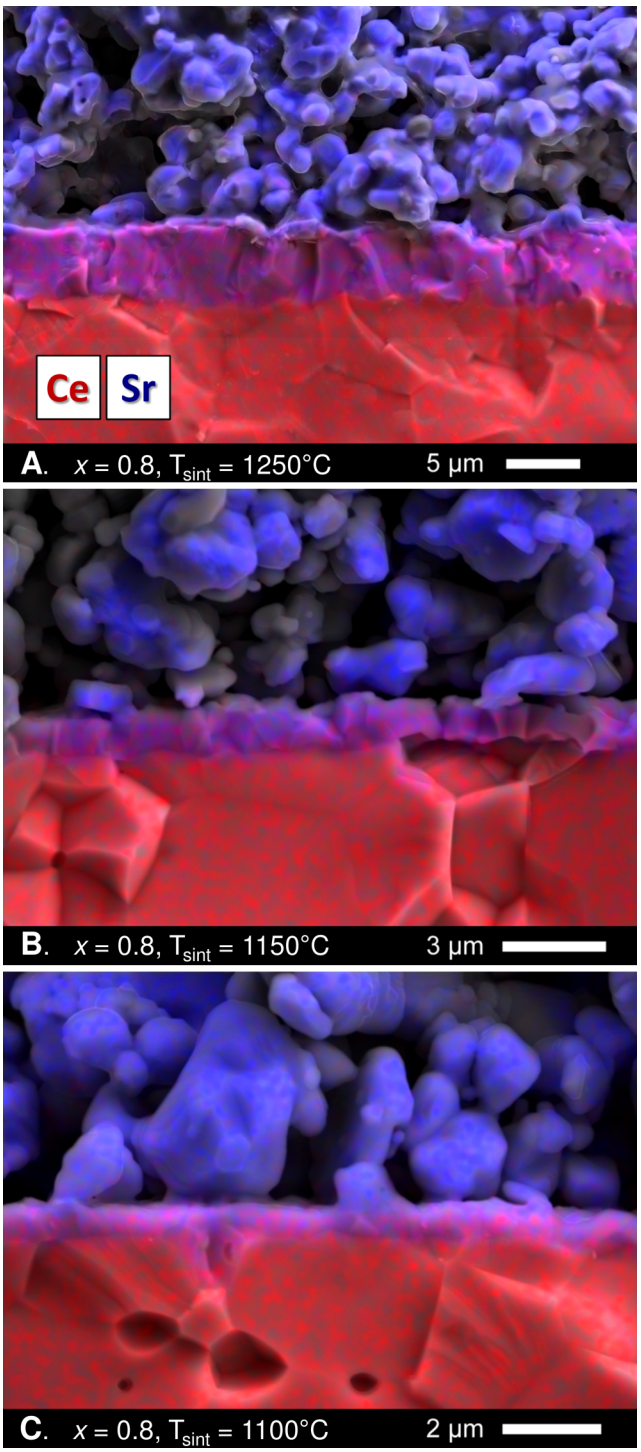

Figure 12. Fractured cross-sections of $(La_{0.2}Sr_{0.8})_2NiO_{4-\delta}$ / CGO10 assemblies sintered at different temperatures: SEM micrographs of near-interface area with overlaid cerium (red) and strontium (blue) EDS elemental mapping. Purple area reveals $SrCeO_3$ layer.

interlayer has a blocking effect on overall electrode process. Decreasing electrode fabrication temperature naturally suppresses the extent of reaction and thickness of cerate layer which decreases from ~ 5µm for T_{sint} = 1250°C to ~ 0.7 µm for electrode sintered at 1100°C (Fig.12 and Fig.11A). For electrodes sintered at 1000°C, the reacted area was not

distinguishable by SEM/EDS, although some reaction between electrode particles and electrolyte surface cannot be excluded (Fig.13). Thus, polarization resistance decreases with decreasing electrode fabrication temperature due to smaller negative effect of electrode/electrolyte reactivity, and achieves minimum for electrode sintered at 1000°C (Fig.11). This is accompanied with a decrease of activation energy of electrode process (Fig.11B and Table S1). Further reduction of sintering temperature to 950°C resulted is some increase of R_η values, but this can be attributed to the fact that this temperature was too low to ensure a good adhesion and mechanical stability of electrode layers. As an illustration of the latter, Fig.S14 demonstrates the cross-section of $(La_{0.2}Sr_{0.8})_2NiO_{4-\delta}$/CGO10 assembly intentionally fractured after the experiment. Even though exfoliation of electrode layer happened, most likely, during the fracture, this typically did not occur with the electrodes sintered at higher temperatures.

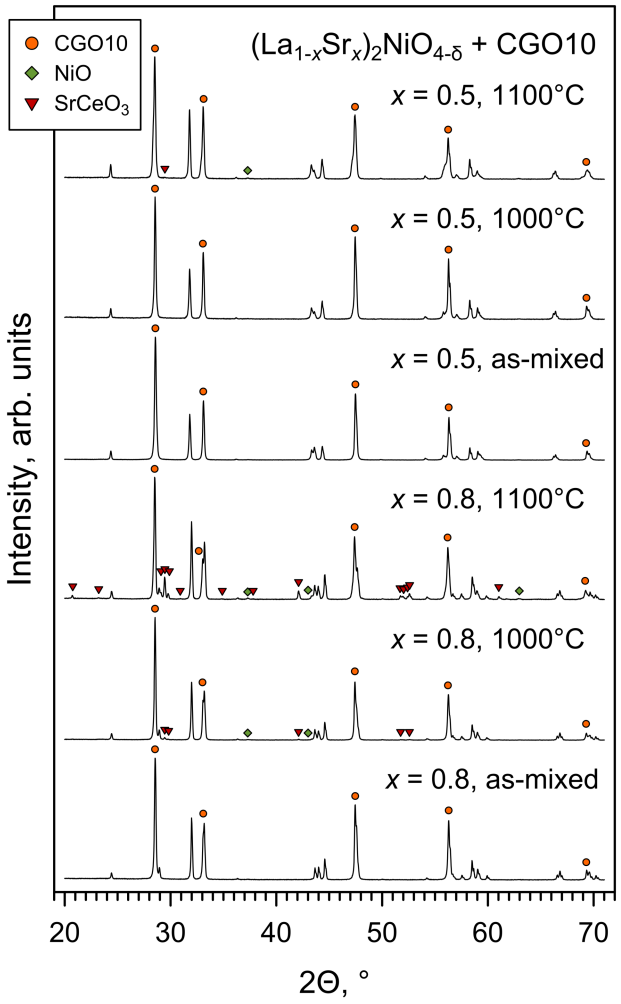

Figure 13. XRD patterns of powdered $(La_{1-x}Sr_x)_2NiO_{4-\delta}$+CGO10 (50:50 wt.%) mixtures, as-mixed and calcined for 10 h at 1000-1100°C in O_2 flow. Reflections of CGO10, NiO and $SrCeO_3$ phases are indexed according to JCPDS PDF #75-0161, #89-7131 and #83-1156, respectively. Unmarked reflections belong to K_2NiF_4-type $(La_{1-x}Sr_x)_2NiO_{4-\delta}$ phase.

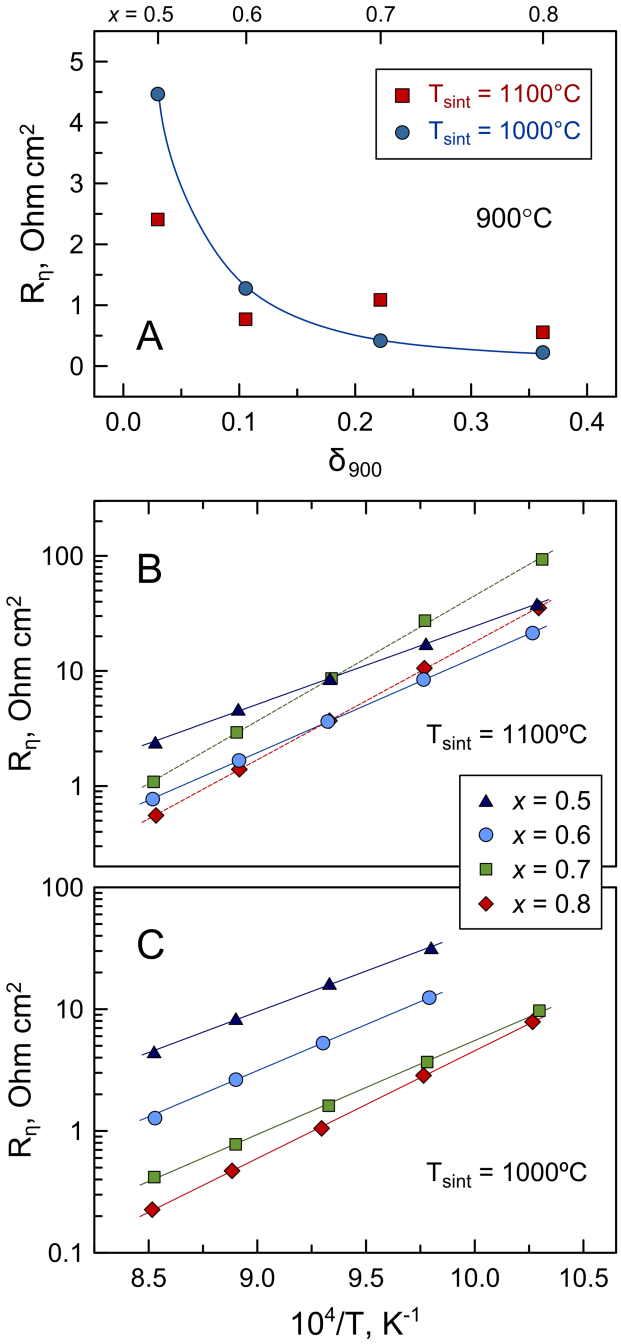

Figure 14. Dependence of polarization resistance of $(La_{1-x}Sr_x)_2NiO_{4-\delta}$ electrodes on oxygen deficiency at 900°C (A); and temperature dependence of polarization resistance of $(La_{1-x}Sr_x)_2NiO_{4-\delta}$ electrodes sintered at 1100°C (B) and 1000°C (C).

Analysis of compositional dependence of polarization resistance of $(La_{1-x}Sr_x)_2NiO_{4-\delta}$ electrodes in contact with CGO10 solid electrolyte (Fig.14) suggests that electrochemical performance in this series is governed by several competing factors. First of all, R_η values expectedly tend to decrease with increasing Sr content and, therefore, with increasing oxygen deficiency (Fig.14A). As discussed above, increasing concentration of oxygen vacancies should increase oxygen-ionic contribution to the total electrical transport, thus improving mixed ionic-electronic conduction

favorable for electrochemical activity of oxide electrodes. Second, increasing strontium content promotes the reactivity between electrode and electrolyte in the course of electrode fabrication (Fig.13), thus having negative effect on the electrode performance. For instance, Li et al. [69] reported that no reaction between La-rich $(La_{0.8}Sr_{0.2})_2NiO_{4\pm\delta}$ and CGO10 occurs at 1100C, while Gong et al. [67] evidenced a "slight" reaction between $(La_{0.8}Sr_{0.2})_2NiO_{4+\delta}$ and SDC electrolyte based on change of lattice parameters. The reactivity between $(La_{1-x}Sr_x)_2NiO_{4-\delta}$ and CGO10 is reflected by activation energy of the electrode process, which increases with x and with sintering temperature (Fig.14(B and C), and Table S1). Another comment is that nickelates with lower strontium content required higher sintering temperature to provide good contact between electrode and electrolyte; this is probably oppositely interrelated with reactivity. This explains why $(La_{1-x}Sr_x)_2NiO_{4-\delta}$ (x = 0.5-0.6) electrodes sintered at 1100°C has lower polarization resistance compared to the same electrodes sintered at 1000°C (Fig.14).

To summarize, increasing oxygen deficiency in Sr-rich nickelates indeed has a positive effect on the electrochemical activity of $(La_{1-x}Sr_x)_2NiO_{4-\delta}$ oxygen electrodes due to anticipated enhanced mixed ionic-electronic transport. These electrodes show however worse electrochemical performance compared to optimized $La_2NiO_{4+\delta}$-based cathodes reported in literature (e.g. Refs.[18,19,46,51]), and this is caused by a strong reactivity with ceria-based solid electrolyte. Future strategies include preparation of nanosized $(La_{1-x}Sr_x)_2NiO_{4-\delta}$ powders in order to decrease the electrode fabrication temperature to ≤ 900°C and thus to minimize the reactivity, and to evaluate the electrochemical behavior of oxygen-deficient nickelates in contact with $(La,Sr)(Ga,Mg)O_{3-\delta}$ (LSGM) solid electrolyte. One may reasonably expect lower reactivity in the latter case.

4. Conclusions

$(La_{1-x}Sr_x)_2NiO_{4-\delta}$ (x = 0.5-0.8) solid solutions were found to preserve K_2NiF_4-type tetragonal structure (space group *I*4/*mmm*) in the studied temperature range (25-1000°C) under oxidizing conditions. Acceptor-type substitution by strontium in these series is compensated by formation of oxygen vacancies and electron-holes. The oxygen deficiency in high-temperature range progressively increases with strontium content and on reducing $p(O_2)$. The concentration of oxygen vacancies in $(La_{0.2}Sr_{0.8})_2NiO_{4-\delta}$ reaches $\delta \sim 0.40$ at 950°C in air and is almost 5 times higher compared to concentration of interstitial oxygen ions in undoped $La_2NiO_{4+\delta}$. K_2NiF_4-type $(La_{1-x}Sr_x)_2NiO_{4-\delta}$ exhibit anisotropic expansion of crystal lattice on heating strongly contributed by chemical expansion. Average TEC values estimated from the high-temperature XRD data increase slightly with strontium substitution and vary in the range $(14.0\text{-}15.4)\times10^{-6}$ K^{-1} at 25-900°C in air. $(La_{1-x}Sr_x)_2NiO_{4-\delta}$ ceramics exhibit *p*-type metallic-like electrical conductivity decreasing on heating and on reducing $p(O_2)$. The highest conductivity, 300 S/cm at 800°C, is observed for x = 0.6 composition. Large oxygen deficiency in Sr-rich compositions implies significant contribution of oxygen-ionic transport to the total conductivity. Polarization resistance of porous $(La_{1-x}Sr_x)_2NiO_{4-\delta}$ electrodes applied onto CGO10 solid electrolyte tends to decrease

with the strontium concentration, in correlation with the concentration of oxygen vacancies in nickelate lattice and anticipated level of mixed ionic-electronic conduction. This is accompanied however with increased reactivity between the electrode and electrolyte materials leading to formation of blocking $SrCeO_3$ layer at the electrode/electrolyte interface. Microstructural optimization is required to decrease electrode fabrication temperature to minimize the negative impact of reactivity on the electrode performance.

Acknowledgements

This work was done within the scope of project IF/01072/2013/CP1162/CT0001 and project CICECO-Aveiro Institute of Materials POCI-01-0145-FEDER-007679 (FCT ref. UID/CTM/50011/2013), financed by national funds through the FCT/MEC and when appropriate co-financed by FEDER under the PT2020 Partnership Agreement. Ekaterina Kravchenko would like to acknowledge the doctoral grant by Belarusian State University and Visby Programme scholarship by Swedish Institute.

Keywords: fuel cells, nonstoichiometric compounds, layered compounds, nickelate, electrode polarization

References

[1] T. Nakamura, K. Yashiro, K. Sato, J. Mizusaki, *Phys. Chem. Chem. Phys.* **2009**, *11*, 3055-3062.

[2] A. Aguadero, M.J. Escudero, M.Pérez, J.A. Alonso, V. Pomjakushin, L. Daza, *Dalton Trans.* **2006**, 4377-4383.

[3] G. Amow, S.J. Skinner, *J. Solid State Electrochem*. **2006**, *10*, 538-546.

[4] A.L. Shaula, E.N. Naumovich, A.P. Viskup, V.V. Pankov, A.V. Kovalevsky, V.V. Kharton, *Solid State Ionics* **2009**, *180*, 812-816.

[5] E. Boehm, J.M. Bassat, P. Dordor, F. Mauvy, J.C. Grenier, Ph. Stevens, *Solid State Ionics* **2005**, *176*, 2717-2725.

[6] S.J. Skinner, J.A. Kilner, *Ionics* **1999**, *5*, 171-174.

[7] S.J. Skinner, J.A. Kilner, *Solid State Ionics* **2000**, *135*, 709-712.

[8] J.B. Smith, T. Norby, *J. Electrochem. Soc.* **2006**, *153*, A233-A238.

[9] A. Tarancón, M. Burriel, J. Santiso, S.J. Skinner, J.A. Kilner, *J. Mater. Chem*. **2010**, *20*, 3799-3813.

[10] R. Sayers, R.A. De Souza, J.A. Kilner, S.J. Skinner, *Solid State Ionics* **2010**, *181*, 386-391.

[11] V.V. Kharton, A.V. Kovalevsky, M. Avdeev, E.V. Tsipis, M.V. Patrakeev, A.A. Yaremchenko, E.N. Naumovich, J.R. Frade, *Chem. Mater*. **2007**, *19*, 2027-2033.

[12] T. Nakamura, K. Yashiro, K. Sato, J. Mizusaki, *Solid State Ionics* **2010**, *181*, 292-299.

[13] A. Flura, S. Dru,C. Nicollet, V. Vibhu, S. Fourcade, E. Lebraud, A. Rougier, J.M. Bassat, J.C. Grenier, *J. Solid State Chem.* **2015**, *228*, 189-198.

[14] V.V. Kharton, A.A. Yaremchenko, E.V. Tsipis, A.A. Valente, M.V. Patrakeev, A.L. Shaula, J.R. Frade and J. Rocha, *Appl. Catal. A* **2004**, *261*, 25-35.

[15] D.C. Zhu, X.Y. Xu, S.J. Feng, W. Liu, C.S. Chen, *Catal. Today* **2003**, *82*, 151-156.

[16] A.A. Yaremchenko, V.V. Kharton, D.O. Bannikov, D.V. Znosak, J.R. Frade, V.A. Cherepanov, *Solid State Ionics* **2009**, *180*, 878-885.

[17] H. Zhao, Q. Li, L.P. Sun, *Sci. China Chem*. **2011**, *54*, 898-910.

[18] T. Ogier, F. Mauvy, J.M. Bassat, J. Laurencin, J. Mougin, J.C. Grenier, *Int. J. Hydrogen Energy* **2015**, *40*, 15885-15892.

[19] B. Philippeau, F. Mauvy, C. Mazataud, S. Fourcade, J.C. Grenier, *Solid State Ionics* **2013**, *249-250*, 17-25.

[20] Y.S. Yoo, M. Choi, J.H. Hwang, H.N. Im, B. Singh, S.J. Song, *Ceram. Int.* **2015**, *41*, 6448-6454.

[21] A. Aguadero, M.J. Escudero, M. Pérez, J.A. Alonso, L. Daza, *J. Fuel Cell Sci. Technol.* **2007**, *4*, 294-298.

[22] E.N. Naumovich, M.V. Patrakeev, V.V. Kharton, A.A. Yaremchenko, D.I. Logvinovich, F.M.B. Marques, *Solid State Sci*. **2005**, *7*, 1353-1362.

[23] E.N. Naumovich, V.V. Kharton, *J. Mol. Struct. THEOCHEM* **2010**, *946*, 57-64.

[24] L. Minervini, R.W. Grimes, J.A. Kilner, K.E. Sickafus, *J. Mater. Chem.* **2000**, *10*, 2349-2354.

[25] W. Xie, Y.L. Lee, Y. Shao-Horn, D. Morgan, *J. Phys. Chem. Lett*. **2016**, *7*, 1939-1944.

[26] A. Chroneos, D. Parfitt, J.A. Kilner, R.W. Grimes, *J. Mater. Chem.* **2010**, *20*, 266-270.

[27] D.E. Rice, D.J. Buttrey, *J. Solid State Chem.* **1993**, *105*, 197-210.

[28] H. Tamura, A. Hayashi, Y. Ueda, *Phys. C* **1996**, *258*. 61-71.

[29] A. Aguadero, J.A. Alonso, M.J. Martínez-Lope, M. T. Fernández-Díaz, M.J. Escudero, L. Daza, *J. Mater. Chem.* **2006**, *16*, 3402-3408.

[30] C.J. Liu, M.D. Mays, D.O. Cowan, M.G. Sánchez, *Chem. Mater.* **1991**, *3*, 495-500.

[31] Y. Takeda, R. Kanno, M. Sakano, O.Yamamoto, M.Takano, Y. Bando, H. Akinaga, K. Takita, J.B. Goodenough, *Mater. Res. Bull*. **1990**, *25*, 293-306.

[32] J.P. Tang, R.I. Dass, A. Manthiram, *Mater. Res. Bull.* **2000**, *35*, 411-424.

[33] R.J. Cava, B. Batlogg, T.T. Palstra, J.J. Krajewski, W.F. Peck Jr., A.P. Ramirez, L.W. Rupp Jr., *Phys. Rev. B* **1991**, *43*, 1229-1232.

[34] M. James, J.P. Attfield, *J. Mater. Chem.* **1996**, *6*, 57-62.

[35] V.V. Vashook, I.I. Yushkevich, L.V. Kokhanovsky, L.V. Makhnach, S.P. Tolochko, I.F. Kononyuk, H. Ullmann, H. Altenburg, *Solid State Ionics* **1999**, *119*, 23-30.

[36] P.J. Heaney, A. Mehta, G. Sarosi, V.E. Lamberti, A. Navrotsky, *Phys. Rev. B* **1998**, *57*, 10370-10378.

[37] X. Granados, J. Fontcuberta, M. Vallet-Regí, M.J. Sayagués, J.M. González-Calbet, *J. Sold State Chem.* **1993**, *102*, 455-464.

[38] M. Khairy, P. Odier, J. Choisnet, *J. Phys. Coll.* **1986**, *47(C1)*, C1-831 - C1-835.

[39] K. Sreedhar, C.N.R. Rao, *Mater. Res. Bull*. **1990**, *25*, 1235-1242.

[40] T. Nakamura, K. Yashiro, K. Sato, J. Mizusaki, *Solid State Ionics* **2009**, *180*, 368-376.

[41] J. Dailly, S. Fourcade, A. Largeteau, F. Mauvy, J.C. Grenier, M. Marrony, *Electrochim. Acta* **2010**, *55*, 5847-5853.

[42] L.V. Makhnach, V.V. Pankov, P. Strobel, *Mater. Chem. Phys*. **2008**, *111*, 125-130.

[43] I.E. Kononyuk, N.G. Surmach, L.V. Makhnach, *Inorg. Mater.* **1982**, *18*, 1029-1031.

[44] V.V. Vashook, S.P. Tolochko, I.I. Yushkevich, L.V. Makhnach, I.F. Kononyuk, H. Altenburg, J. Hauck, H. Ullmann, *Solid State Ionics* **1998**, *110*, 245-253.

[45] E. Kravchenko, D. Khalyavin, K. Zakharchuk, J. Grins, G. Svensson, V. Pankov, A. Yaremchenko, *J. Mater. Chem. A* **2015**, *3*, 23852-23863.

[46] Y. Shen, H. Zhao, J. Xu, X. Zhang, K. Zheng, K. Świerczek, *Int. J. Hydrogen Energy* **2014**, *39*, 1023-1029.

[47] T. Inprasit, P. Limthongkul, S. Wongkasemjit, *J. Electrochem. Soc.* **2010**, *157*, B1726-B1730.

[48] Z. Li, R. Haugsrud, T. Norby, *Solid State Ionics* **2011**, *184*, 42-46.

[49] Z. Li, R. Haugsrud, J.B. Smith, T. Norby, *J. Electrochem. Soc*. **2009**, *156*, B1039-B1044.

[50] K. Kammer, *Ionics* **2009**, *15*, 325-328.

[51] Y.P. Wang, Q. Xu, D.P. Huang, K. Zhao, M. Chen, B.H. Kim, *Int. J. Hydrogen Energy* **2016**, *41*, 6476-6485.

[52] B. Guan, W. Li, H. Zhang, X. Liu, *J. Electrochem. Soc*. **2015**, *162*, F707-F712.

[53] E.Yu. Pikalova, N.M. Bogdanovich, A.A. Kolchugin, D.A. Osinkin, D.I. Bronin, *Proc. Eng*. **2014**, *98*, 105-110.

[54] J.E. Millburn, M.A. Green, D.A. Neumann, M.J. Rosseinsky, *J. Solid State Chem.* **1999**, *145*, 401-420.

[55] J. Gopalakrishnan, G. Colsmann, B. Reuter, *J. Solid State Chem.* **1977**, *22*, 145-149.

[56] H.A.J. Thomas, R. Stevens, *Br. Ceram. Trans. J.* **1989**, *88*, 144-151.

[57] M. Tomczyk, A.M. Senos, P.M. Vilarinho, I.M. Reaney, *Scripta Mater*. **2012**, *66*, 288-291.

[58] W. Höland, G.H. Beall, *Glass-Ceramic Technology, Second Edition*, Wiley, Hoboken, NJ, **2012**; pp. 304-307.

[59] K. Ishikawa, S. Kondo, H. Okano, S. Suzuki, Y. Suzuki, *Bull. Chem. Soc. Jpn.* **1987**, *60*, 1295-1298.

[60] V.V. Vashook, N.E. Trofimenko, H. Ullmann, L.V. Makhnach, *Solid State Ionics* **2000**, *131*, 329-336.

[61] A.R. Cleave, J.A. Kilner, S.J. Skinner, S.T. Murphy, R.W. Grimes, *Solid State Ionics* **2008**, *179*, 823-826.

[62] C. Tealdi, C. Ferrara, P. Mustarelli, M. Saiful Islam, *J. Mater. Chem*. **2012**, *22*, 8969-8975.

[63] D. Marrocchelli, S.R. Bishop, H.L. Tuller, B. Yildiz, *Adv. Funct. Mater*. **2012**, *22*, 1958-1965.

[64] D. Marrocchelli, N.H. Perry, S.R. Bishop, *Phys. Chem. Chem. Phys*. **2015**, *17*, 10028-10039.

[65] A.A. Yaremchenko, S.M. Mikhalev, E.S. Kravchenko, J.R. Frade, *J. Eur. Ceram. Soc.* **2014**, *34*, 703-715.

[66] A.C. Tomkiewicz, M. Tamimi, A. Huq, S. McIntosh, *J. Mater. Chem. A* **2015**, *3*, 21864-21874.

[67] M. Gong, L. Lu, H. Zhang, L. Gao, Y. Guo, J. Jin, *Mater. Res. Bull*. **2009**, *44*, 1630-1634.

[68] I. Kosacki, H.L. Tuller, *Solid State Ionics* **1995**, *80*, 223-229.

[69] Q. Li, Y. Fan, H. Zhao, L.H. Huo, *Chin. J. Inorg. Chem*. **2006**, *22*, 2025-2030.

10.1002/cssc.201601340

Table of Contents

Deficiency promotes electrochemistry: Oxygen nonstoichiometry, electrical properties and electrochemical activity of Sr-rich $(La_{1-x}Sr_x)_2NiO_{4-\delta}$ were studied for use as oxygen electrodes of solid oxide fuel/electrolysis cells. Increasing strontium content is demonstrated to increase oxygen deficiency thus promoting mixed ionic-electronic conductivity and decreasing polarization resistance of $(La_{1-x}Sr_x)_2NiO_{4-\delta}$ electrodes.